Journal of Vacuum Science and Technology B

RESEARCH ARTICLE | DECEMBER 23 2024

Filtering the beam from an ionic liquid ion source

Special Collection: Papers from the 67th International Conference on Electron, Ion and Photon Beam Technology and Nanofabrication (EIPBN 2024)

Alexander C. G. Storey ; Aydin Sabouri ; Rohit Khanna ; Usama Ahmed ; Carla Sofia Perez-Martinez

J. Vac. Sci. Technol. B 42, 064201 (2024)
https://doi.org/10.1116/6.0004029

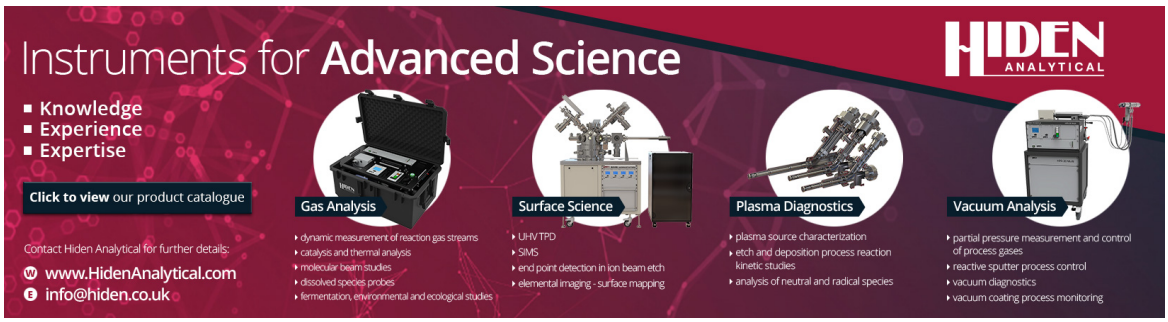

JVST B
Journal of Vacuum Science & Technology B

ARTICLE

pubs.aip.org/avs/jvb

Filtering the beam from an ionic liquid ion source

Cite as: J. Vac. Sci. Technol. B 42, 064201 (2024); doi: 10.1116/6.0004029
Submitted: 30 August 2024 · Accepted: 3 December 2024 ·
Published Online: 23 December 2024

Alexander C. G. Storey, Aydin Sabouri, Rohit Khanna, Usama Ahmed, and Carla Sofia Perez-Martinez[a)]

AFFILIATIONS

London Centre for Nanotechnology, University College London, London, WC1H 0AH, England

Note: This paper is part of the Special Topic Collection: Papers from the 67th International Conference on Electron, Ion and Photon Beam Technology and Nanofabrication (EIPBN 2024).

[a)]**Author to whom correspondence should be addressed:** carla.perezmartinez@ucl.ac.uk

ABSTRACT

Ionic liquid ion sources (ILIS) have been proposed as a source of alternative ion chemistries for surface etching, focused ion beams, and secondary ion mass spectrometry. These ion sources produce polydisperse ion beams containing several solvated ion species with a distribution of energies, and it is necessary to filter the ion beam to obtain monoenergetic beams with a single ion chemistry as required by nanomanufacturing and analytical applications. In this work, a Wien filter has been designed, built, and tested for use with an ILIS using the liquid 1-ethyl-3-methylimidazolium tris(pentafluoroethyl)trifluorophosphate, or EMI-FAP. COMSOL MULTIPHYSICS simulations have been used to validate the design. The full and unfiltered ion beams have been characterized using time-of-flight mass spectrometry and retarding potential analysis, and these measurements confirm that the filter is effective in isolating monomer ions from heavier ion species in the beam.

I. INTRODUCTION

Ionic liquid ion sources (ILIS) are point sources of ions that rely on field evaporation from room-temperature molten salts. ILIS have been proposed for use in space propulsion technology[1] and in material processing, including surface etching,[2] focused ion beams,[3] and secondary ion mass spectrometry.[4,5] There are many ionic liquids available for use in ILIS, and they give access to a plethora of positively and negatively charged ion chemistries, including simple halides (Cl^-, I^-), organic molecules, and fluorinated species (BF_4^-, PF_6^-). ILIS have already been used to etch semiconductor materials, including Si,[2,6–15] SiO_2,[7] glass,[7,14,15] GaN, and gold.[6] The etching yields measured from ILIS indicate that the beams can achieve enhanced etching thanks to the reactivity of the ions in the beam; for example, the beam from EMI-BF_4 can remove eight atoms of Si per incident ion at a modest energy of 7 keV,[6] compared to typical yields of 2–3 atoms per incident ion for beams of noble gases or metals at higher energies of 30 keV.[16] However, further development is required for the use of ILIS in nanomanufacturing. Previous material irradiation investigations have used the full beam from the ion source, but the full beam is polydisperse with ions of different masses and energies. The intended material applications require monoenergetic beams with specific ion species to ensure process integrity and to enhance the focusing capabilities of the beam. Monodisperse beams are of particular relevance for lithography, high-resolution imaging, and quantum applications.[17–22] In this work, a Wien filter is designed and implemented to isolate distinct species of the beam from an ILIS based on the liquid 1-ethyl-3-methylimidazolium tris(pentafluoroethyl)trifluorophosphate, or EMI-FAP. The full and unfiltered beams are characterized using time-of-flight (TOF) spectrometry and retarding potential analysis (RPA) to confirm that the filter is effective in separating the ion species.

Previous work indicates that the full beam from ILIS contains ions of different masses and energies.[23–25] For an ion source using an ionic liquid comprising a cation A^+ and anion B^-, operating in the positive polarity, the beam includes ions of the form $(AB)_kA^+$, where k usually takes values of 0 (monomers), 1 (dimers), and 2 (trimers). Oligomers of a higher order are less common. The situation is similar in the negative mode, only the ions are of the form $(AB)_kB^-$.

The solvated ions can fragment into a lighter ion and a neutral cluster, either in the acceleration zone between the emitter and the extractor, or once the oligomer has been fully accelerated. These ion fragments have a range of energies. Let V_0 be the potential of the emitter and consider the extractor to be at zero potential. Ideally, ions will be accelerated to a full kinetic energy of qV_0. If an

ion of mass m_p and charge q breaks up into an ion of mass m_f and a neutral cluster, at a potential αV_0 ($0 \leq \alpha \leq 1$), the resulting kinetic energy of the charged fragment is given by

$$K_f = \frac{m_f}{m_p} q(V_0 - \alpha V_0) + q\alpha V_0. \quad (1)$$

Thus, the ion beam contains not only monomers, dimers, and trimers that were generated at the emission site and are fully accelerated to a kinetic energy qV_0, but also lighter ions resulting from fragmentation events that have energies ranging from $\frac{m_f}{m_p} qV_0$ ($\alpha = 0$, field-free fragmentation after exiting the extractor) to qV_0 ($\alpha = 1$, fragmentation just after emission). A Wien filter can be used to select specific masses and reduce the energy spread of the ILIS ion beam. Wien filters are routinely used with liquid metal alloy ion sources (LMAIS), both in commercially available systems and in the development of new LMAIS.[26–32] This work explores the effectiveness of a Wien filter in separating not only monomers from dimers in an ILIS beam, but also the highly energetic monomers from fragmented species.

The simulations used to model the Wien filter are described in Sec. II. Then, the experimental method, including source preparation, filter operational details, and RPA and TOF setup, is described in Sec. III. Experimental results are included in Sec. IV, and a summary and conclusion are presented in Sec. V.

II. MODELING

COMSOL MULTIPHYSICS simulations were used to evaluate the performance of different filter configurations in selecting only high energy monomeric species and maximizing the proportion of fully accelerated monomers exiting the filter.

The simulated model consists of an Einzel lens, a Wien filter, and electrostatic deflectors. These elements are presented in Fig. 1. The ion source is placed at the origin and the beam travels along the x-axis. The Einzel lens is composed of three cylindrical electrodes, with the central electrode biased to a high potential and the outer electrodes grounded. The lens controls the ion trajectories and affects the current density. The Wien filter incorporates electrostatic deflectors and permanent magnets to generate uniform and perpendicular magnetic and electric fields. The filter's magnetic field is aligned with the y-axis, while the filter's electric field is aligned with the z-axis. The filter acts as a velocity selector: ideally, only particles that have an axial velocity matching the ratio of the magnitudes of the electric to the magnetic field will be undeflected through the filter, and particles with different velocities are deflected and blocked by an exit aperture. In practice, the electric and magnetic fields generated by the filter are not perfectly uniform and may leak out of the device, and some additional deflectors are included in the test designs to correct for these imperfections. These deflectors are also useful for beam alignment corrections.

Most of the geometrical dimensions of the lens, filter, and deflectors were kept fixed, guided by the size of commercially available Neodymium magnets and space constraints. A parametric sweep was used in COMSOL to measure the monomer and dimer yields as four test parameters were changed, namely, the voltage of

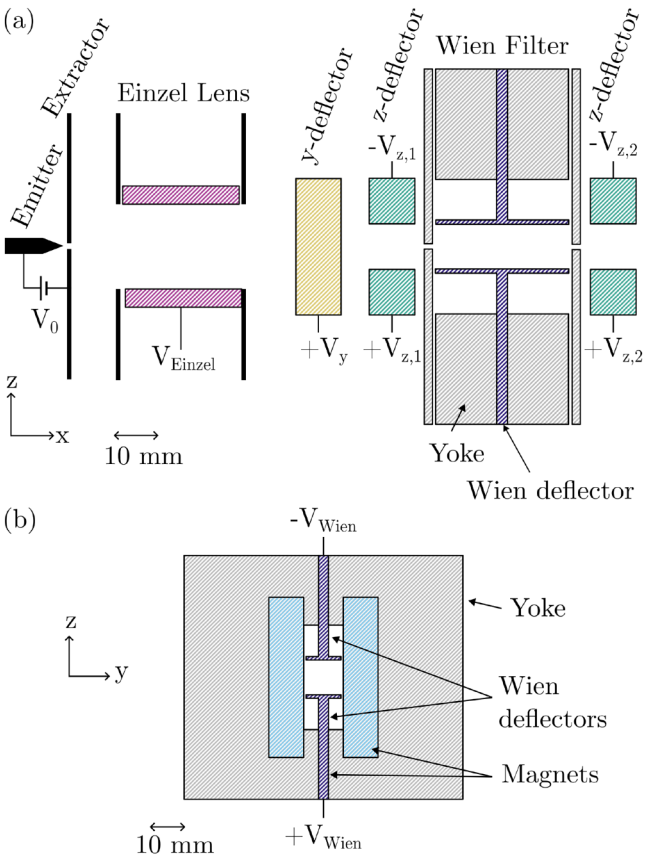

FIG. 1. Geometry of the lens, deflector, and Wien filter setup used to filter the beam from an ionic liquid ion source. (a) The emitter is biased at a potential V_0 with respect to an extractor aperture. The beam passes through a cylindrical Einzel lens to direct the ion beam, then through deflectors to correct beam trajectories, and then enters the Wien filter. The figure shows the cross section of the filter through the x–z plane, with the electric field from the Wien deflectors pointing in the z-direction. The magnets are not visible in this cross section. (b) Cross section of the Wien filter along the y–z plane. Two permanent magnets are held by an iron yoke, with the magnetic field pointing along the y-direction, and the electrostatic deflectors placed in the gap between the magnets.

the Einzel lens central electrode, V_{Einzel}, the voltage of the z-deflector preceding the lens, $V_{z,1}$, the voltage of the Wien filter deflectors, V_{Wien}, and the radius of the Wien filter entrance aperture, r_a. To evaluate each design, the three dimensional electric and magnetic fields produced by the lens, filter, and deflectors are solved from Maxwell's equations using the finite element method, assuming steady-state and no space charge. Ions are produced from a single point at the origin, and their initial velocity distribution is modeled based on experimental data from the literature. The COMSOL charged particle tracing module is used to calculate the positions and velocity vectors $\mathbf{v}$ of ions as they travel through the electric field $\mathbf{E}$ and the magnetic field $\mathbf{B}$, and they experience the Lorentz force $\mathbf{F} = q(\mathbf{E} + \mathbf{v} \times \mathbf{B})$. Finally, the number of ions of each type arriving to the filter exit plane is extracted from the simulation.

The angular distribution of ions from an ILIS has been investigated,[33–35] and the distribution has been found to be between a parabola and a super-Gaussian. For simplicity, the model assumes a parabolic ion distribution with a beam half-angle of 18°.[33] For each ion species and energy, ten thousand ions are initialized at $t = 0$ at the origin. The initial velocity of each ion is determined by assuming a total kinetic energy of $\alpha q V_0$ and by assigning a polar and azimuthal angle to each ion with respect to the emission axis. The inverse transform method[36] is used to recover a representative sample of polar angles from the parabolic distribution from randomly generated values between 0 and 1. The azimuthal angle for each ion is picked at random from a uniform distribution.

The geometry and the materials of the ion optics are as follows. First, the Einzel lens entrance is at $x = 10$ mm. The electrodes are all stainless steel. Along the x-direction, the entrance, mid and exit electrodes are 1, 26, and 1 mm long, and separated from each other by a 1 mm gap. The inner diameter of the cylindrical electrodes is 19 mm.

The Wien filter entrance is located 40 mm away from the exit of the lens. The Wien filter uses two commercially available N42 sintered Neodymium magnets (Magnet Expert Ltd.). The magnets are 30 mm long in the x-direction, 46 mm tall in the z-direction, and 10 mm thick in the y-direction, with the magnetization aligned with the y-axis. The magnets are held in a low carbon steel yoke, with the magnet separation set arbitrarily at 11 mm. The filter deflectors are two stainless steel plates, 30 mm long in the x-direction, 10 mm wide in the y-direction, and separated by 10 mm along the z-direction. The yoke is enclosed by two aperture plates, which each are 2 mm long in the x-direction. The exit aperture has a radius of 0.5 mm, and the entrance aperture is subject to change in the simulations.

Two sets of stainless steel deflector plates are placed between the lens and the filter. The plates are 30 mm by 10 mm, placed 10 mm apart, and are placed so that they apply a field along 10 mm of the beam path. The first set of deflector plates applies a voltage V_y to generate a field in the y-direction and is used for beam alignment corrections. The second set of deflector plates applies an electric field in the z-direction to correct for beam bending due to leakage of the magnetic field outside of the Wien filter.

The ray tracing results indicate that it is indeed possible to separate the monomer from the dimer ions using this filter configuration for operation voltages of $V_0 = \pm 1200$ V. Tables summarizing the results from the parametric sweep, listing the yields of monomer and dimer ions as a function of V_{Einzel}, $V_{z,1}$, V_{Wien}, and r_a, are provided in the supplementary material. In the positive mode, the highest yield of fully accelerated monomers was 27.1%, when $V_{\text{Einzel}} = 1173$ V, $V_{z,1} = 60$ V, $V_{\text{Wien}} = 278$ V, and r_a is 0.45 mm. At these conditions, no dimers exit the filter. Figure 2(a) illustrates the results from ray tracing of EMI^+ monomers for these settings. Ions with off-axis trajectories are redirected by the Einzel lens to the Wien filter. A slight trajectory correction is applied by the z-deflector immediately before the entrance of the Wien filter. Although several trajectories impact the exit plate, a fraction of the trajectories leaves the filter. Figures 2(b) and 2(c) show the locations of the positive monomers and dimers as they impact the innermost surface of the exit aperture plate. In the negative mode, the highest yield of monomers was 21.8%, when $V_{\text{Einzel}} = -1161$ V, $V_{z,1} = 28$ V, $V_{\text{Wien}} = 140$ V, and r_a is 0.45 mm. In this case, no negative dimers exit the filter. Figures 2(d) and 2(e) show the locations of the monomers and dimers as they impact the innermost surface of the exit aperture plate for these conditions.

Simulations were also run for monomers resulting from dimer fragmentation. As the energy of the fragments decreases, the likelihood of a fragment exiting the filter goes down, and only positive fragments with $\alpha \geq 0.82$ can progress through the filter. In the negative mode, fragments with $\alpha \geq 0.72$ can progress.

III. EXPERIMENTAL METHODS

Experimental details for the ion source and ion optics are explained in Subsection III A. Two main characterization techniques are used to investigate the properties of the full and filtered ion beams. Time-of-flight mass spectrometry (TOF-MS) is explained in Subsection III B, and RPA is described in Subsection III C. The TOF-MS and RPA instruments are similar to the designs proposed by Miller.[24,37]

A. Ion source, lens, and filter

The ILIS emitter is laser milled from porous glass with 1 μm pore size into a needle with a height of 300 μm and a tip radius of curvature of approximately 5 μm. A scanning electron micrograph of the tip of the emitter is presented in Fig. 3.

To load the emitter with ionic liquid, the emitter is installed upon a linear stage placed above a small crucible filled with EMI-FAP (Merck, high purity) within a vacuum chamber. The system is evacuated to pressures below 1×10^{-6} mbar for a few hours, to degas and dry the ionic liquid, and then the emitter is submerged into the ionic liquid for at least 12 h. The loaded emitter is lifted out of the liquid prior to venting. The emitter is installed in a teflon mount alongside a distal electrode made of porous carbon xerogel (ca. 1 μm pore diameter). The tip is then centered in front of a 1.5 mm diameter aperture in a stainless steel extractor plate. A Matsusada AP-3B1(A)-L bipolar voltage amplifier provides potential to the needle emitter, while the extractor is held at ground. The current emitted by the ILIS is monitored using a circuit developed *in house*, which uses an optocoupler to measure the response of a diode. The diode is connected in series to the power supply and shines in proportion to the emitted current; this arrangement is necessary to electrically isolate the current measurement at high voltage.

The Einzel lens potential is provided by a Matsusada AP-3B1 (A)-L. The Wien filter electrostatic deflectors are biased by an EMCO F30CT, with equal magnitude positive and negative voltage supplied to each electrode. The ancillary y- and z-deflectors are biased using GW Instek GPD-3303D power supplies. A GM07 Gaussmeter (Hirst Magnetic Instruments) was used to measure the magnetic field at the center of the filter (0.647 T) as well as the leaking fields at the entrance and exit aperture (magnitude 0.112 T). All high-voltage measurements were calibrated with the Keysight 10076C oscilloscope probe.

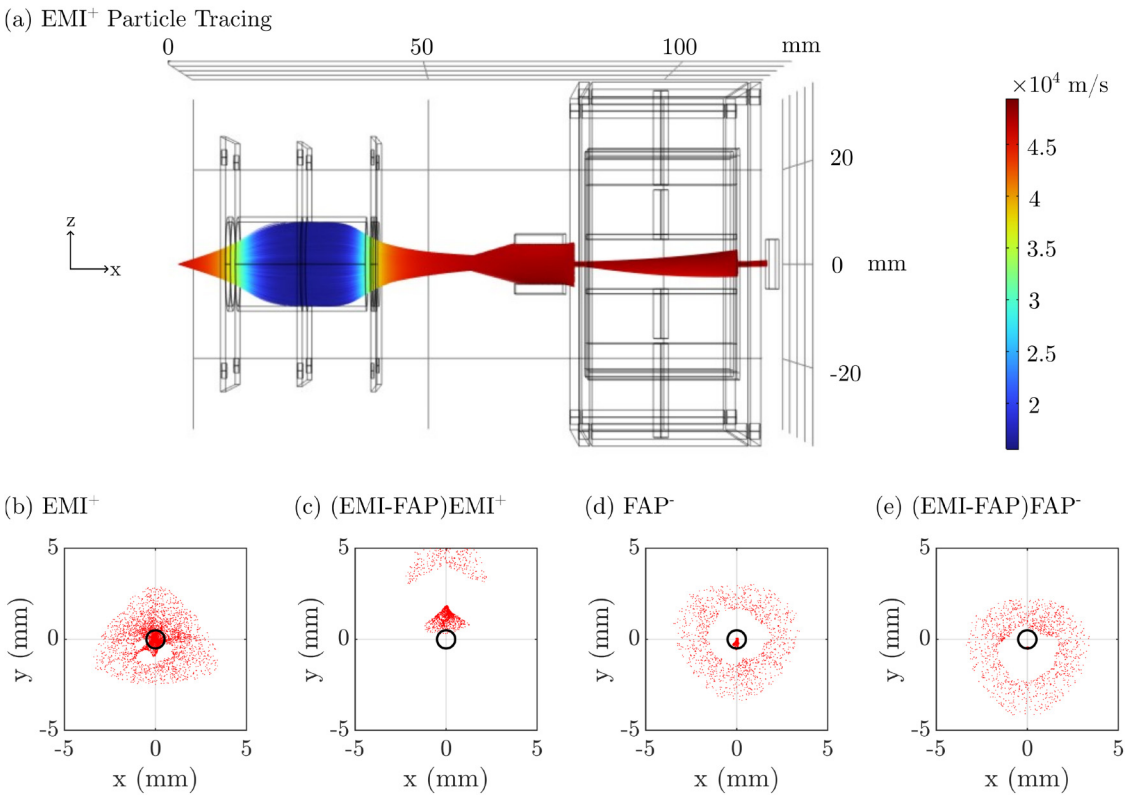

FIG. 2. COMSOL simulations of filtering ion optics for an ionic liquid ion source using the liquid EMI-FAP at $V_0 = \pm 1200$ V. All results are for fully accelerated ions. (a) EMI^+ ray tracing. Ions are emitted from the origin in the left. The plot shows a line for each ion, with the line changing color with the ion speed as indicated by the colorbar. Ions are directed by the Einzel lens toward the Wien filter, with a trajectory correction applied by the z-deflectors immediately preceding the filter. Several ion trajectories exit the filter. (b)–(d) Poincaré maps illustrating the location of ions as they impact the inner surface of the exit aperture plate. Panels (b), (c), (d), and (e) show the results for EMI^+, $(EMI\text{-}FAP)EMI^+$, FAP^-, and $(EMI\text{-}FAP)FAP^-$, respectively. A significant fraction of monomer ions travels through the center of the aperture, but in the case of dimers, all ions impact the inner surfaces of the aperture and none can exit the filter.

B. Time-of-flight mass spectrometry

TOF-MS measures the composition of ion beams by providing information about the mass-to-charge ratios of the component species. TOF-MS involves creating high frequency pulses of the ion beam, which are measured by a current collector. A schematic of the setup is shown in Fig. 4. A deflection gate periodically applies a field to the ion beam. When the gate is on, no ions arrive to the collector, and when the gate is switched off, the lightest ions will arrive first, causing a spike in measured current on the collector. The arrival of heavier (slower) ions further increases the current, until the full beam's current is collected. The ions present can be identified by their flight times across a known distance according to the following equation:

$$t = L\sqrt{\frac{m}{2qV_0}}, \tag{2}$$

where L is the flight length, V_0 is the voltage applied to the emitter, m is the mass, and q is the charge of the species. This equation assumes that all ions are fully accelerated to the applied potential V_0.

The TOF gate consists of two grounded stainless steel entrance apertures with a diameter of 6 mm, followed by two stainless steel deflectors, 2.4 mm long and placed 6 mm apart. Voltages of +800 and −800 V are periodically applied to the deflectors via a custom-built pulse generator circuit which is controlled by a Keysight 33500B signal generator, thus creating a field that deflects the beam away from the detector. The pulses used for these measurements were set at 1 kHz. The current collector was a Channeltron Photonis Magnum 4900, whose output was measured using an optically isolated oscilloscope probe (Micsig SigOFIT MOIP200P, 200 MHz model) to provide galvanic isolation as the channeltron outputs are floating to up to ±3 kV. The output signal was recorded using a Keysight DSOX3024T oscilloscope with signal averaging mode ON, to average 2000 cycles.

C. Retarding potential analyzer

A spherical RPA is used to determine the energies of the ions in the beam. The setup is shown in Fig. 4. This instrument consists of a grounded entrance grid, a retarding grid, and a secondary

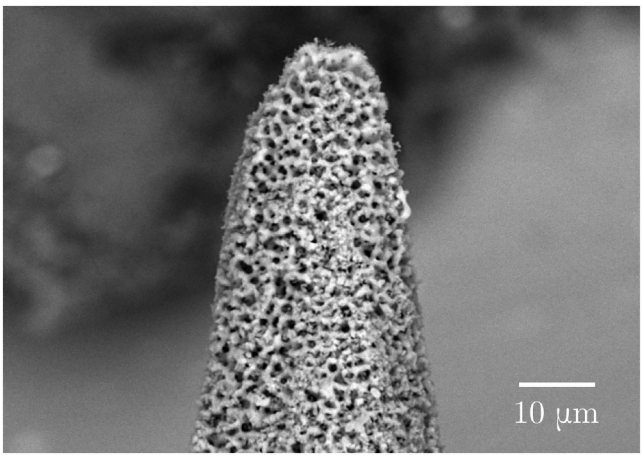

FIG. 3. Scanning electron micrograph of the dry porous emitter tip used in this work. The tip is laser micromachined to achieve a radius of curvature below 10 μm.

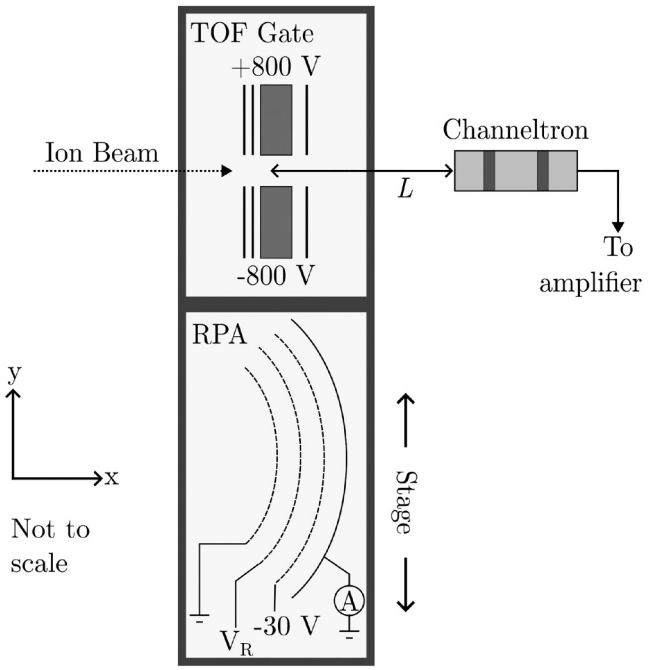

FIG. 4. Setup schematic for TOF and RPA measurements. The TOF instrument consists of a gate that periodically interrupts the ion beam away from a channeltron collector, placed a distance L away from the gate. The current output from the channeltron detector is directed to an amplifier and oscilloscope. By measuring the flight time of the particles, it is possible to determine the mass composition of the ion beam. The TOF gate and RPA are mounted on a vacuum-compatible stage, so that the measurement can be changed while remaining in vacuum. The RPA consists of three spherical grids followed by a spherical cap collector. The first grid is grounded, the second grid applies a retarding potential V_R, and the last grid applies a potential of -30 V to suppress the spurious secondary electron emission from the spherical cap as it is impacted by ions. The collected current is measured as a function of V_R to determine the energy distribution of ions in the beam.

electron suppression grid, placed in front of a current collector. The retarding grid potential is ramped between 0 V and a voltage slightly higher than V_0, while measuring the collected current. Particles will be stopped when the retarding potential V_R exceeds their kinetic energy, and so the changes in the current can be used to determine the beam's energy distribution.

The three grids are shaped into spherical caps. Each grid is constructed using a scaffold stainless steel hexagonal grid on which a tungsten mesh is welded. The effective permeability of all grids is 34.3%. A stainless steel spherical cap collector with radius of curvature of 100 mm is mounted behind the grids. The instrument has a spherical shape so that when the ion source is placed exactly at the center of the sphere, there will be no artificial spreading in the RPA curves. However, if the ion source is not in this ideal location, ions traveling off-axis will be stopped by slightly different potentials than ions traveling on-axis, and some amount of spreading will occur.

The retarding grid is biased by a Matsusada AP-3B1(A)-L, which is controlled with a Keysight signal generator 33500B, and the secondary electron grid is provided -30 V by a GW Instek GPD-3303D power supply. The current collected by the RPA is measured using a Keithley 6485 picoammeter. The signals for collected current and V_R are recorded using a Keysight DSOX3024T oscilloscope in high resolution mode.

The RPA and TOF deflectors are mounted on a Standa 8MT175V-200 stage, so that the measurement can be changed while remaining in vacuum. The chamber is evacuated to pressures of below 1×10^{-6} mbar for all emission experiments.

Experiments with the filtered beam have the Einzel lens, Wien filter, and all deflectors in place, so that the distance between the emitter and the gate is 262 mm, and the TOF distance is $L = 956.5$ mm. The RPA collector is 270 mm away from the emitter. For full beam measurements, the Einzel lens and Wien filter are removed, but some of the deflectors are left in place for beam alignment corrections. In this case, the distance between the emitter and the gate is 187 mm, the flight distance is $L = 1036.5$ mm, and the RPA collector is 196 mm away from the emitter.

IV. EXPERIMENTAL RESULTS

Stable emission was obtained for both the positive and negative polarity, with operation voltage magnitudes in the range of 1200 V. The Wien filter was implemented as described in Sec. II, with the exception that it was necessary to remove the entrance aperture due to alignment issues.

TOF experiments indicate that the filter is effective in removing dimers and higher order oligomers from the ion beam and creating a pure beam of monomers. Figure 5 shows TOF measurements of the full and filtered ion beam in both the positive and negative polarities, with three sample voltages explored in each polarity. In the figure, the x-axis has been converted from time to mass using Eq. (2), assuming singly charged ions with energy qV_0,

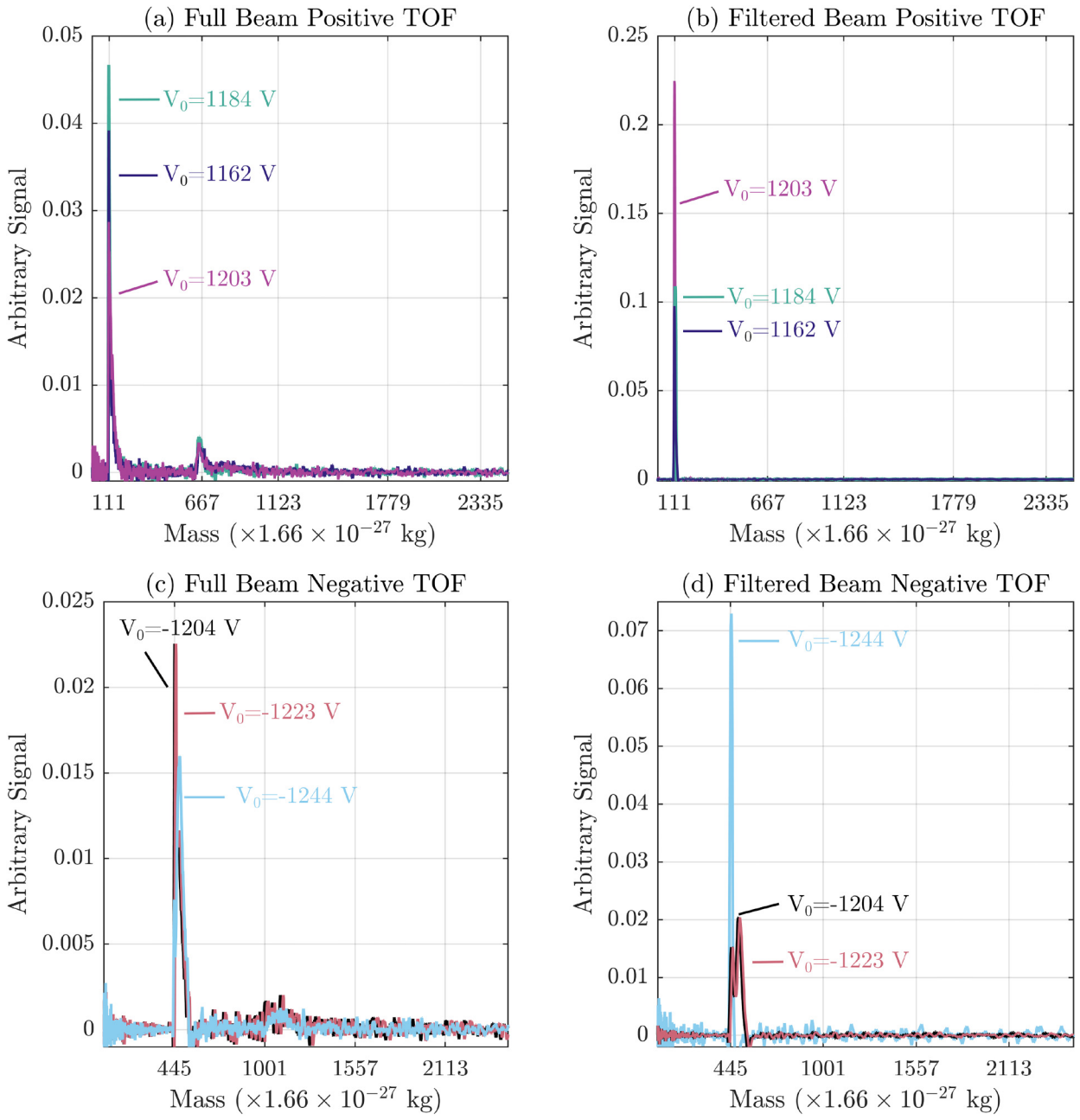

FIG. 5. Time-of-flight spectrometry measurements of the full and filtered beam from the ionic liquid EMI-FAP. (a) Full and (b) filtered beam measurements for $V_0 = 1162$, 1184, and 1203 V. (c) Full and (d) filtered beam measurements for $V_0 = -1204$, -1223, and -1244 V. Peaks in the full beam signal are observed at the masses expected for the monomer and dimer ions, with some spread around these peaks due to ion fragments from heavier ions. The filtered beams only show peaks in signals at the monomer mass and zero signal at higher masses. Full details of the setup settings for each measurement are included in the supplementary material.

and the y-axis shows the derivative of the current signal as a function of ion mass. The derivative has been smoothed with a low-pass Savitzky-Golay filter. Figures 5(a) and 5(b) show the results of experiments in the positive mode, for the full and filtered beams, respectively. Figures 5(c) and 5(d) show the results of experiments in the negative mode, for the full and filtered beams, respectively. The raw TOF current data as a function of time are included in the supplementary material.

The full beam TOF experiments demonstrate the presence of solvated ions. For the full beam in the positive mode, clear peaks are present at masses of 111 and 667 amu, which correspond to the monomer EMI^+ and dimer (EMI-FAP)EMI^+, respectively. The signal from masses greater than 667 amu is indicative of ion fragments originating from trimer ions [$(EMI\text{-}FAP)_2EMI^+$, 1123 amu]. In contrast, the filtered beam TOF data only show a sharp peak at the monomer mass. The full beam in the negative mode shows signatures of the monomer and dimer ions [FAP^-, 445 amu, and (EMI-FAP)FAP^-, 1001 amu], as well as traces of slower ions that correspond to fragmentation from trimer ions [$(EMI-FAP)_2FAP^-$, 1557 amu]. The filtered beam data only shows peaks close to the monomer mass.

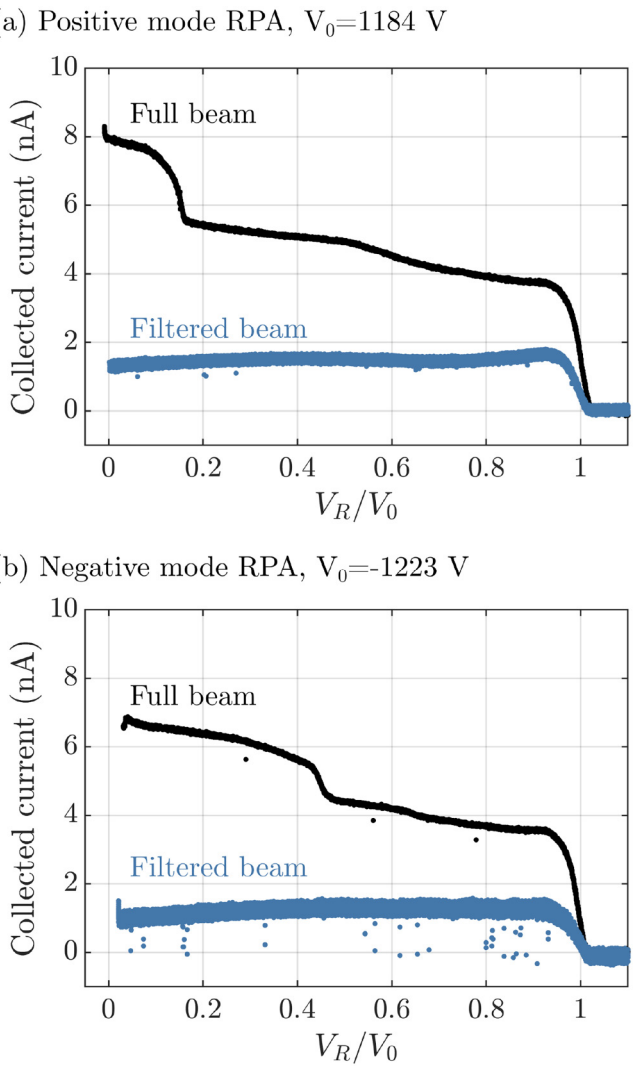

FIG. 6. Retarding potential analyzer measurements for the full and filtered beams from EMI-FAP, for (a) positive and (b) negative mode. Full beam measurements are shown in black, and filtered measurements in blue. Full details of the setup settings for each measurement are included in the supplementary material.

The TOF results are supported by RPA experiments. RPA measurements of the full and filtered beams are shown in Fig. 6, plotting the collected current as a function of V_R/V_0. Ideally, if the beam were monoenergetic, the current would stay constant as V_R/V_0 is swept from 0 to 1 and drop sharply to zero when $V_R/V_0 = 1$. However, decreases in current in the RPA curves for $V_R/V_0 < 1$ are observed due to ion fragmentation.

The full beam data for $V_0 = 1184$ V are shown in Fig. 6(a) and display signatures of fully accelerated and fragmented ions. The largest current drop just below $V_0/V_R = 1$ corresponds to ions that have been accelerated close to the full acceleration potential. There are two steps in current at approximately $V_0/V_R = 0.17$ and 0.54. As per Eq. (1), the fragmentation of positive dimers (667 amu) into monomers (111 amu) in the field-free region ($\alpha = 0$) gives ions with a kinetic energy of $111/667qV_0 = 0.17qV_0$. Similarly, the 0.54 step correponds to field-free trimer to dimer fragmentation. Furthermore, the constant drop in current between $V_0/V_R = 0.17$ and 1 is due to fragmentation in the acceleration region. There is some artificial spreading on the data resulting from the nonideal placement of the RPA detector.

The RPA data for the filtered beam, also plotted in Fig. 6(a), present a much simpler scenario, with only ions accelerated close to the full acceleration potential leaving the filter. The filtered beam has a flat RPA profile until approximately $V_0/V_R = 0.9$, showing that most of the low-energy fragments have been removed from the beam.

The filter is also effective in negative mode operation. Figure 6(b) shows the RPA results for the full and filtered beam for an operation voltage of $V_0 = -1223$ V. The full beam profile has a sharp drop in current just below $V_0/V_R = 1$, corresponding to ions that have been accelerated close to the applied potential. There is also a clear step close to $V_0/V_R = 0.47$ (dimer to monomer fragmentation with $\alpha = 0$) and another smaller step close to $V_0/V_R = 0.67$ (trimer to dimer fragmentation with $\alpha = 0$). The full beam data also show the steady decrease in current indicative of fragmentation in the acceleration region. The filtered beam (blue curve) has a relatively flat profile until approximately $V_0/V_R = 0.9$, indicating that, as in the positive mode, most of the fragments have been removed by the filter.

V. SUMMARY AND OUTLOOK

A Wien filter with ancillary ion optics has been used to isolate monomer ions from an ionic liquid ion source. COMSOL MULTIPHYSICS simulations were used to evaluate the design of the filter. The characteristics of the full and filtered ion beams from the ionic liquid 1-ethyl-3-methylimidazolium tris(pentafluoroethyl)trifluorophosphate were measured using TOF and RPA. Full beam profiles show a polydisperse ion beam with monomers, dimers, trimers, and quadrumers, as well as fragmented ions. When the beam is filtered, only signatures corresponding to monomer ions are observed, and no solvated ions appear to exit the filter. Future work includes using the filter with other ionic liquids, and taking advantage of this setup to compare the effects of individual ion species on sample irradiation as opposed to the full beam. This work should

help inform the design of ILIS devices for material treatment applications.

SUPPLEMENTARY MATERIAL

See the supplementary material for the tables summarizing the results of the COMSOL parametric sweeps, an example COMSOL simulation of ray tracing of the negative ion FAP^-, a summary of the experimental settings for RPA and TOF measurements, the TOF experimental data plotted as a function of flight time instead of ion mass, and an estimation of the Wien filter resolution.

ACKNOWLEDGMENTS

This research was supported by a UKRI Future Leaders Fellowship (No. MR/S032312/1) and a EPSRC DTP Studentship for Alexander Storey (Nos. EP/T517793/1 and EP/R513143/1).

AUTHOR DECLARATIONS

Conflict of Interest

Dr. Carla Sofia Perez-Martinez is co-inventor on U.S. patent 9704685, pertaining to ionic liquid ion source technology, and for which she receives royalties.

Author Contributions

Alexander C. G. Storey: Data curation (lead); Formal analysis (lead); Investigation (lead); Methodology (supporting); Software (lead); Validation (lead); Visualization (lead); Writing – original draft (equal); Writing – review & editing (supporting). **Aydin Sabouri:** Investigation (supporting); Methodology (supporting); Resources (supporting); Software (supporting); Supervision (supporting); Writing – review & editing (equal). **Rohit Khanna:** Investigation (supporting); Methodology (supporting); Resources (supporting); Writing – review & editing (supporting). **Usama Ahmed:** Data curation (supporting); Formal analysis (supporting); Investigation (supporting); Software (supporting); Writing – original draft (supporting); Writing – review & editing (supporting). **Carla Sofia Perez-Martinez:** Conceptualization (lead); Data curation (supporting); Formal analysis (supporting); Funding acquisition (lead); Investigation (supporting); Methodology (lead); Project administration (lead); Software (supporting); Supervision (lead); Validation (supporting); Visualization (supporting); Writing – original draft (equal); Writing – review & editing (lead).

DATA AVAILABILITY

The data that support the findings of this study are available from the corresponding author upon reasonable request.

REFERENCES

[1]D. Krejci, F. Mier-Hicks, R. Thomas, T. Haag, and P. Lozano, J. Spacecr. Rockets **54**, 447 (2017).
[2]C. Perez-Martinez, S. Guilet, N. Gogneau, P. Jegou, J. Gierak, and P. Lozano, J. Vac. Sci. Technol. B **28**, L25 (2010).
[3]A. N. Zorzos and P. C. Lozano, J. Vac. Sci. Technol. B **26**, 2097 (2008).
[4]Y. Fujiwara and N. Saito, Rapid Commun. Mass Spectrom. **32**, 1867 (2018).
[5]Y. Fujiwara and N. Saito, J. Vac. Sci. Technol. A **39**, 063218 (2021).
[6]C. S. Perez-Martinez, "Engineering ionic liquid ion sources for ion beam applications," Ph.D. thesis (Massachusetts Institute of Technology, 2016).
[7]T. Xu, Z. Tao, and P. C. Lozano, J. Vac. Sci. Technol. B **36**, 052601 (2018).
[8]R. Yoshida, M. Hara, H. Oguchi, T. Suzuki, and H. Kuwano, in *27th IEEE International Conference on Micro Electro Mechanical Systems (MEMS)*, San Francisco, CA, 26–30 January 2014 (IEEE, New York, 2014), pp. 463–466.
[9]R. Yoshida, M. Hara, H. Oguchi, and H. Kuwano, in *28th IEEE International Conference on Micro Electro Mechanical Systems (MEMS)*, Estoril, Portugal, 18–22 January 2015 (IEEE, New York, 2015), pp. 93–96.
[10]R. Yoshida, M. Hara, H. Oguchi, and H. Kuwano, J. Vac. Sci. Technol. B **34**, 022001 (2016).
[11]N. V. Chinh, L. V. Minh, T. Ono, and H. Kuwano, in *Proceedings of the 9th Symposium on Micro-Nano Science and Technology*, Sapporo, Hokkaido, Japan, 30 October–1 November 2018 (The Japan Society of Mechanical Engineers, 2018), p. 31pm2PN88.
[12]N.-V. Chinh, L.-V. Minh, T. Ono, and H. Kuwano, in *20th International Conference on Solid-State Sensors, Actuators and Microsystems and Eurosensors XXXIII (TRANSDUCERS AND EUROSENSORS XXXIII)*, Berlin, Germany, 23–27 June 2019 (IEEE, New York, 2019), pp. 1674–1677.
[13]N. V. Chinh, L. V. Minh, T. Ono, and H. Kuwano, in *34th IEEE International Conference on Micro Electro Mechanical Systems (MEMS)*, Gainesville, FL, 25–29 January 2021 (IEEE, New York, 2021), pp. 14–17.
[14]M. Takeuchi, Y. Hoshide, T. Hamaguchi, H. Ryuto, and G. H. Takaoka, Trans. Mater. Res. Soc. Jpn. **40**, 87 (2015).
[15]M. Takeuchi, Y. Hoshide, H. Ryuto, and G. H. Takaoka, J. Vac. Sci. Technol. A **34**, 02D108 (2016).
[16]S. Tan, R. Livengood, D. Shima, J. Notte, and S. McVey, J. Vac. Sci. Technol. B **28**, C6F15 (2010).
[17]M. Sutula *et al.*, Nat. Mater. **22**, 1338 (2023).
[18]I. B. Harris *et al.*, PRX Quantum **4**, 040301 (2023).
[19]X. Xu *et al.*, Nanophotonics **12**, 485 (2023).
[20]N. Delegan, S. J. Whiteley, T. Zhou, S. L. Bayliss, M. Titze, E. Bielejec, M. V. Holt, D. D. Awschalom, and F. J. Heremans, Nanotechnology **34**, 385001 (2023).
[21]A. M. Jakob *et al.*, Adv. Mater. **34**, 2103235 (2022).
[22]R. Acharya *et al.*, Commun. Mater. **5**, 57 (2024).
[23]P. Lozano, J. Phys. D: Appl. Phys. **39**, 126 (2006).
[24]C. E. Miller and P. C. Lozano, Appl. Phys. Lett. **116**, 254101 (2020).
[25]M. Schroeder, X. Gallud, E. Petro, O. Jia-Richards, and P. C. Lozano, J. Appl. Phys. **133**, 173303 (2023).
[26]L. Bischoff, P. Mazarov, L. Bruchhaus, and J. Gierak, Appl. Phys. Rev. **3**, 021101 (2016).
[27]K. Höflich *et al.*, Appl. Phys. Rev. **10**, 041311 (2023).
[28]M. Titze *et al.*, AIP Adv. **14**, 045326 (2024).
[29]M. Titze, D. L. Perry, E. A. Auden, J. L. Pacheco, J. B. S. Abraham, and E. S. Bielejec, J. Vac. Sci. Technol. B **39**, 012802 (2021).
[30]V. Chandrasekaran, M. Titze, A. R. Flores, D. Campbell, J. Henshaw, A. C. Jones, E. S. Bielejec, and H. Htoon, Adv. Sci. **10**, 2300190 (2023).
[31]A. Melnikov, T. Gerya, M. Hillmann, I. Kamphausen, W. Oswald, P. Stauche, R. Wernhardt, and A. Wieck, Nucl. Instrum. Methods Phys. Res., Sect. B **195**, 422 (2002).
[32]L. Bischoff, Ultramicroscopy **103**, 59 (2005).
[33]P. Lozano and M. Martínez-Sánchez, J. Colloid Interface Sci. **282**, 415 (2005).
[34]C. S. Perez-Martinez and P. C. Lozano, J. Vac. Sci. Technol. B **30**, 06F601 (2012).
[35]E. M. Petro, X. Gallud, S. K. Hampl, M. Schroeder, C. Geiger, and P. C. Lozano, J. Appl. Phys. **131**, 193301 (2022).
[36]S. M. Ross, "Generating continuous random variables," in *Simulation*, 6th ed., edited by S. M. Ross (Academic, Boston, 2023), pp. 69–98.
[37]C. E. Miller, "Characterization of ion cluster fragmentation in ionic liquid ion sources," Ph.D. thesis (Massachusetts Institute of Technology, 2019).